Process Safety and Environmental Protection 142 (2020) 370–379

Contents lists available at ScienceDirect

Process Safety and Environmental Protection

journal homepage: www.elsevier.com/locate/psep

Determination on the hazard zone of spontaneous coal combustion in the adjacent gob of different mining stages

Li Ma[a,b,*], Ruizhi Guo[a,b,*], Mingming Wu[c], Weifeng Wang[a,b], Lifeng Ren[a,b], Gaoming Wei[a,b]

[a] *School of Safety Science and Engineering, Xi'an University of Science and Technology, Xi'an, 710054, China*
[b] *Shaanxi Key Laboratory of Prevention and Control of Coal Fire, Xi'an, 710054, China*
[c] *Ordos City Yingpanhao Coal Industry Co., Ltd, Ordos City 017000, China*

ARTICLE INFO

Article history:
Received 18 December 2019
Received in revised form 14 June 2020
Accepted 18 June 2020
Available online 24 June 2020

Keywords:
Narrow pillar
Spontaneous coal combustion
Adjacent gob
Oxygen concentration
Numerical simulation

ABSTRACT

Coal seam mining, especially during roadway driving with narrow coal pillars, can cause air leakage along the gob side and increase the risk of spontaneous coal combustion. To explore the oxygen distribution and spontaneous coal combustion risk zone in an adjacent gob of a fully mechanized mining face, a temperature-programmed experiment, a secondary oxidation experiment, gas monitoring, and numerical simulation were conducted. The oxygen consumption rates of the coal sample in primary and secondary oxidation processes were compared, and the oxygen concentration at the inner coal pillar of an adjacent gob was monitored. The oxygen concentration distribution in the adjacent gob was simulated, and the spontaneous coal combustion risk zone in the adjacent gob was determined. The results show that secondary coal oxidation was stronger than primary oxidation below 90 °C, and primary coal oxidation was stronger than secondary oxidation above 90 °C. The oxygen consumption rate ratio (i.e., the oxidation size) of the coal sample during primary and secondary oxidation processes below 90 °C was fitted to obtain the relationship. During roadway driving of the 2202 working face along the gob, the air leakage intensity of the coal pillar was between 0.0335–0.0365 $cm^3/(s\cdot cm^2)$. The area 23 m from the coal pillar to the depth of the adjacent gob behind the heading face was found to be at risk of spontaneous coal combustion. During normal and end mining of the 2202 working face, the air leakage intensity of the coal pillar along the gob was between 0.005–0.024 $cm^3/(s\cdot cm^2)$. The residual coal in a narrow area, 87 m long in the adjacent gob was in an oxidizing environment. When the working face advanced slowly, the residual coal in this area was prone to oxidation and at risk of spontaneous combustion.

1. Introduction

In China, many coal mines face the threat of coal fire disasters, and the outlook is not optimistic. Coal fire can produce large amounts of toxic and harmful gases which threaten the work safety of miners (Bai et al., 2020a). More seriously, coal fire can cause huge economic losses and environmental damage. (Su et al., 2017; Querol et al., 2011). Twenty-five major coal mining provinces, with more than 130 large and medium-sized coal mines, are threatened by spontaneous coal combustion to varying degrees (Kuenzer et al., 2007; Wessling et al., 2010). From 2004 to 2015, 87 coal fire accidents caused a total of 661 deaths in China (Zheng et al., 2019). India, the United States, South Africa, Australia, Indonesia, and other countries have also been plagued by coal fire disasters (Ma et al., 2019). The gob is a key area for coal fires, and the prevention and control of spontaneous coal combustion in gobs is particularly important (Huang et al., 2018; Lei et al., 2018).

Mine ventilation provides fresh airflow for miners to breathe, dilutes toxic and harmful gases, and improves the underground climate for a good working environment (Cheng and Yang, 2012; Widiatmojo et al., 2015). Even with ventilation, air leakage frequently occurs due to the crushing and falling of coal, poor design of the ventilation structure, and poor sealing. Air leakage is one of the main causes of spontaneous combustion of residual coal in the gob, stop line, and coal pillar (Wu and Liu, 2011; Yuan and Smith, 2012; Yang et al., 2014; Tang et al., 2016). When air leakage provides adequate oxygen, residual coal undergoes coal-oxygen complexation

* Corresponding authors at: School of Safety science and Engineering, Xi'an University of Science and Technology, Xi'an, 710054, China.
E-mail addresses: mal@xust.edu.cn (L. Ma), grz20180326@163.com (R. Guo).

https://doi.org/10.1016/j.psep.2020.06.035
0957-5820/

Nomenclature

C	oxygen concentration, %
C_0	oxygen concentration in the fresh airflow, mol·cm^{-3}
C_1	oxygen concentration in the inlet of the coal sample tank, mol·cm^{-3}
C_2	oxygen concentration in the outlet of the coal sample tank, mol·cm^{-3}
c	actual oxygen concentration, mol/cm^3
c_0	standard oxygen concentration, c_0=9.375 × 10^{-6} mol/cm^3
D	oxygendiffusion coefficient, m^2/s
g	gravitationalacceleration, m/s^2
ΔH^{CO}	reaction heat of and CO, kJ/mol
ΔH^{CO_2}	reaction heat of CO_2, kJ/mol
ΔH^r	58.8 kJ/mol
K	permeability coefficient, m^3·s/kg
k	absolute permeability
L	coal sample height, cm
P	air leakage pressure, Pa
p	porosity, %
Q	air leakage intensity, cm^3/(cm^2·s)
$\overline{Q}$	gas supply, cm^3/s
Q_x	air leakage intensity component in X direction
Q_y	air leakage intensity cVomponent in Y direction
Q_z	air leakage intensity component in Z direction
$q_{max}(T)$	the maximum heat release rate, J/cm^3·s
$q_{min}(T)$	the minimum heat release rate, J/cm^3·s
S	tank bottom area, cm^2
T	temperature, °C
V_1	oxygen consumption rate of primary oxidation, mol/(cm^3·s)
V_2	oxygen consumption rate of secondary oxidation, mol/(cm^3·s)
$V(T)$	oxygen consumption rate, mol/(cm^3·s)
$V_0(T)$	oxygen consumption rate in the fresh airflow, mol/(cm^3·s)
$V^0_{CO}(T)$	standard CO production rate, mol/(cm^3·s)
$V^0_{CO}2(T)$	standard CO_2 production rate, mol/(cm^3·s)
$v_0(\theta)$	oxygen consumption rate when the temperature is θ, mol/(cm^3·s)
x	the coordinates in the loose coal body of the roadway, cm
x_0	the coordinates in the surface of the roadway, cm
$\bar{x}$	coal temperature, °C
$\bar{y}$	the ratio of V_1 and V_2

Greek Symbol

ρ	oxygen density, kg/m^3
μ	air viscosity coefficient, kg/(m·s)
I	calculation model in roadway driving along gob
II	calculation model in normal mining
III	calculation model in end mining

through physical adsorption, chemical adsorption, and chemical reaction. In a suitable heat storage environment, heat accumulation induced by coal oxidation leads to spontaneous coal combustion (Bai et al., 2020b; Deng et al., 2018b; Xi et al., 2017). Air leakage may lead to accelerated coal oxidation, an increased heating rate, and an enlarged high-temperature area. As a result, the time needed for spontaneous combustion of coal is greatly reduced (Song et al., 2014). Many scholars have investigated the influence of air leakage on spontaneous coal combustion, the laws of gas production during spontaneous coal combustion, and the determination of spontaneous coal combustion risk zones in gob (Zhou et al., 2019).

The ventilation mode mainly depends on the coal mining method. Due to different layouts of the working face and roadway, the ventilation mode can change. The development of narrow coal pillar mining technology has not only improved the coal recovery rate, but also maintains the stability of the surrounding rock in the roadway along the gob. Air leakage into the gob through coal pillar cracks is also an important consideration (Lu and Qin, 2015). After roadway driving along the gob, the initial equilibrium state of the stress is changed, leading to redistribution of the mine stress (Gao et al., 2014). Cracks appear in the upper coal pillar, allowing air leakage, which can lead to spontaneous coal combustion. Moreover, it takes a significant amount of time to pass through the roadway, causing loose and residual coal in the adjacent gob to be exposed to conditions conducive to spontaneous coal combustion. The loose coal beside the roadway along the gob and residual coal in the adjacent gob are at risk of coal fire.

During the spontaneous combustion of coal, oxygen is continuously consumed, and specific gas products are generated (Ren et al., 2019; Li et al., 2018). The composition, content, growth rate, ratio, and other indicators of self-combustion coal products can be used to assess the stage of development of spontaneous coal combustion (Liang et al., 2019). The oxygen consumption rate, CO generation rate, various gas ratios, and fire coefficient are used to predict spontaneous coal combustion (Zhu et al., 2012; Wang et al., 2018; Liu and Qin, 2017a; Guo et al., 2019).

Many scholars have studied the risk zone of spontaneous coal combustion in gob. The indicators of spontaneous combustion of residual coal in the gob are oxygen concentration distribution (Deng et al., 2018a), wind speed distribution (Zhuo et al., 2019), CO emissions (Liu and Qin, 2017a), and temperature change (Huang et al., 2018). With the development of numerical simulation technology, simulation of spontaneous combustion of residual coal in the gob has changed from a two-dimensional model to a three-dimensional model (Shi et al., 2019), from a single physical field to a multi-physical coupling simulation (Rosema et al., 2001), from fixed coordinates to moving coordinates (Liu and Qin, 2017b).

Till date, most studies have focused on the spontaneous combustion of residual coal in a single gob (i.e. the gob of the working face), while adjacent gobs have not been considered. Spontaneous coal combustion in an adjacent gob is different from spontaneous coal combustion in other areas. The residual coal in an adjacent gob will be affected by coal mining activities twice. The adjacent gob is directly or indirectly connected to the new working face gob, and residual coal in the adjacent gob undergoes secondary oxidation or even multiple oxidations (Deng et al., 2016a, 2016b). After residual coal undergoes oxidation, its microstructure and surface structure is changed, thus affecting the oxidation degree, and increasing the risk of fire (Tang and Wang, 2019).

The purpose of this paper is to investigate the risk zones of spontaneous coal combustion of adjacent gobs in the three mining stages, and achieve early prediction, which is conducive to underground environment protection and safety production. Through primary and secondary oxidation experiments, the oxygen consumption rate and heat release rate of coal samples in the new gob and adjacent gob were obtained. The oxygen consumption rate was used as the basis for setting numerical simulation parameters. Models with an adjacent gob were established to simulate the oxygen distribution during roadway driving along the gob, normal mining, and end mining. Risk zones of spontaneous coal combustion in adjacent gob were determined by the oxygen consumption rate measured experimentally, the oxygen concentration observed in the field, and the oxygen concentration distribution numerically simulated. This paper provides a certain reference for the early prediction of spontaneous coal combustion in adjacent gob.

Table 1
Coal sample size and experimental conditions for temperature-programmed experiment.

Coal sample Number	Granularity (mm)	Coal weight (g)	Air flow (ml/min)	Heating rate (°C/min)
Mixed sample	0~10	250	30	0.5

Table 2
Proximate analyses of the coal samples.

sNOR	Mad(%)	Ad(%)	Vdaf (%)	FC_{ad} (%)
Bituminous coal	5.69	9.06	38.39	46.86

2. Overview of working face

The average elevations of a coal mine ground and working face in a 2-2 coal seam are 1244.9 m and 523 m, respectively. A 2-2 coal seam has a simple structure, an average inclination of 3°, and an average thickness of 6.3 m. A 2-2 coal seam is mainly composed of non-caking coal, with small amounts of long flame coal and slightly caking coal. The 2201 and 2202 working faces of the Yingpanhao coal mine are adjacent working faces. The 2201 gob is located south of the 2202 auxiliary transport roadway. There is a 5 m wide protective coal pillar between the 2202 auxiliary transport roadway and the 2201 gob. The layout of the 2202 working face and 2201 gob is shown in Fig. 1.

3. Materials and methods

3.1. Spontaneous coal combustion characteristics experiment

3.1.1. Experimental conditions

Coal samples from a 2-2 coal seam of the Yingpanhao coal mine were crushed and sieved into particle sizes of 0–0.9 mm, 0.9–3 mm, 3–5 mm, 5–7 mm, and 7–10 mm. A mixed sample was made using 50 g of each of the five particle sizes. Coal sample size and experimental conditions for the temperature-programmed experiment are shown in Table 1.

Ash, moisture, volatile carbon, and fixed carbon of coal samples were obtained through proximate analysis. Proximate analyses of the coal samples are shown in Table 2.

3.1.2. Experimental device

The temperature-programmed experimental system consists of five parts: a gas supply system, a coal sample tank, an intelligent temperature control system, a gas collection system, and an analysis system. The experimental system is shown in Fig. 2. The gas in the cylinder was of standard airflow with 21 % oxygen and 79 % nitrogen. After flowing through the preheated copper pipe, the airflow passed through the bottom of the coal sample tank and reacted with the coal sample. The gas generated by the reaction was collected through the outlet above the coal sample tank. To eliminate other gaseous impurities in the spontaneous coal combustion process, the standard airflow was introduced to the reactor at a steady flow rate of 30 mL/min for 20 min. The coal samples were then heated steadily from 30 °C to 180 °C, and data were recorded at intervals of 10 °C. The gas supply and heating rate were constant at 30 mL/min and 0.5 °C/min, respectively. The collected gases were analyzed using a gas chromatograph with a minimum accuracy of 0.1 ppm.

The operation procedure for secondary oxidation was as follows: after primary oxidation the coal sample was cooled to room temperature under nitrogen conditions, then sealed and stored. Using the same procedure as in the primary oxidation, the coal sample was oxidized again.

3.2. Gas monitoring in gob

To monitor the gas content and concentration along the gob side as accurately as possible, 49 boreholes were drilled through the narrow coal pillar into the adjacent gob, with a distance between boreholes of 50 m. The drilling depth was just enough to penetrate the coal pillar. The boreholes were 1.5–2.0 m from the bottom plate. A 2 in. steel tube with a bundle tube was inserted into each borehole to monitor the gas in the adjacent gob. The drilling arrangement of roadway driving along the gob of the 2202 working face is shown in Fig. 3.

3.3. Oxygen distribution in adjacent gob

3.3.1. Calculation model

The geometries and mesh of the model are generated by ANSYS 15.0 workbench design modeler and mesh tool, respectively. The calculation models in three mining stages of the 2202 working face, roadway driving along the gob, normal mining, and end mining were selected and named as Models I, II, and III, respectively. The size of the calculation model was determined according to actual field size. The height of residual coal in the two crossheadings of the gob and the middle area of the gob was set to 1.5 m and 1 m, respectively. The height of the calculation model was set to 10 m. The calculation model of the adjacent gob in three mining stages of the 2202 working face is shown in Fig. 4.

3.3.2. Simulation parameter

To facilitate the numerical simulation calculations, the following hypotheses were made: the gob is regarded as a uniform and isotropic porous medium region consisting of the residual coal and the upper overburden. The seepage caused by airflow in the residual coal and the upper overburden will not change its density (Liang and Wang, 2017). When the airflow passes through the porous medium, laminar flow occurs in the gob due to the small airflow velocity, and its momentum equation is in accordance with Darcy's law (Pan et al., 2011). Air leakage in the gob occurred only in fractured coal and rock mass. Then the governing equations are as follows (Zhai et al., 2011, 2019):

$$\frac{\partial Q_x}{\partial x} + \frac{\partial Q_y}{\partial y} + \frac{\partial Q_z}{\partial z} = 0 \tag{1}$$

$$\begin{cases} Q_x = -\dfrac{K_x}{\rho g}\dfrac{\partial P}{\partial x} \\ Q_y = -\dfrac{K_y}{\rho g}\dfrac{\partial P}{\partial y} \\ Q_z = -\dfrac{K_z}{\rho g}\dfrac{\partial P}{\partial z} \end{cases} \tag{2}$$

$$\frac{\partial}{\partial x}\left(\frac{K_x}{\rho g}\frac{\partial P}{\partial x}\right) + \frac{\partial}{\partial y}\left(\frac{K_y}{\rho g}\frac{\partial P}{\partial y}\right) + \frac{\partial}{\partial z}\left(\frac{K_z}{\rho g}\frac{\partial P}{\partial z}\right) = 0 \tag{3}$$

$$Q_x \cdot \frac{\partial C}{\partial x} + Q_y \cdot \frac{\partial C}{\partial y} + Q_z \cdot \frac{\partial C}{\partial z} = D_x \cdot \frac{\partial^2 x}{\partial x^2} + D_y \cdot \frac{\partial^2 y}{\partial y^2} + D_z \cdot \frac{\partial^2 z}{\partial z^2} - V(T) \tag{4}$$

$$V(T) = V_0(T) \cdot \frac{C}{C_0} \tag{5}$$

where coordinate axes are represented by x, y, and z, and Q represents the air leakage intensity. Q_x, Q_y, and Q_z indicate the air

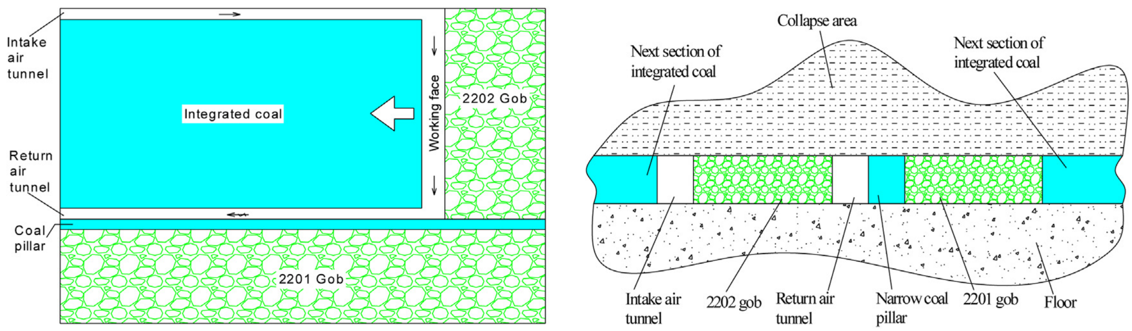

(a) (b)

Fig. 1. Layout of 2202 working face and 2201 gob.

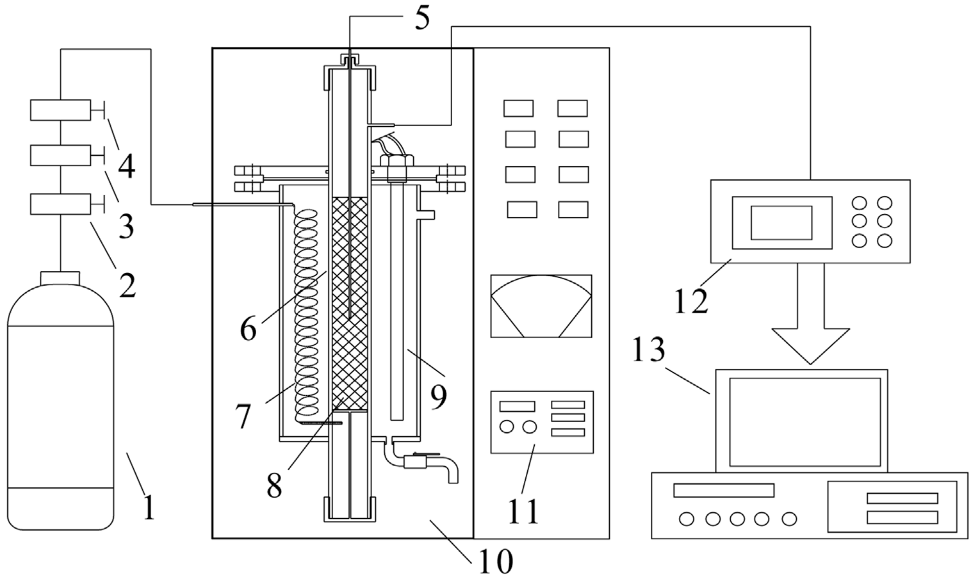

1. Experimental gas 2. Pressure reducing valve 3. Regulator valve 4. Flow meter 5.Platinum wire temperature probe 6.Coal sample tank 7.Preheat brass 8.Coal sample 9.Blender 10.Temperature-programmed oven 11.Control panel 12.Gas chromatography 13.Computer

Fig. 2. Schematic of the temperature-programmed experimental system.

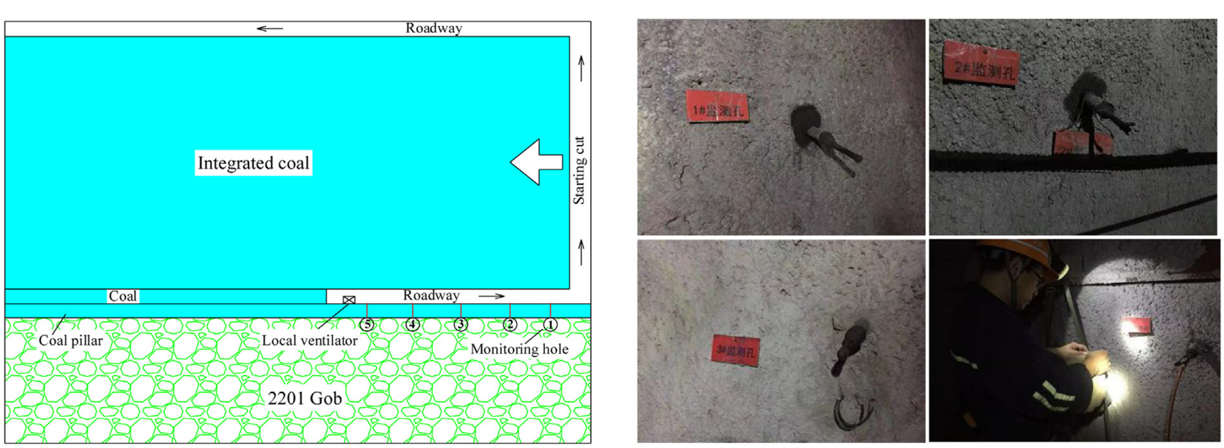

(a) (b)

Fig. 3. 2202 Drilling layout during roadway driving along gob.

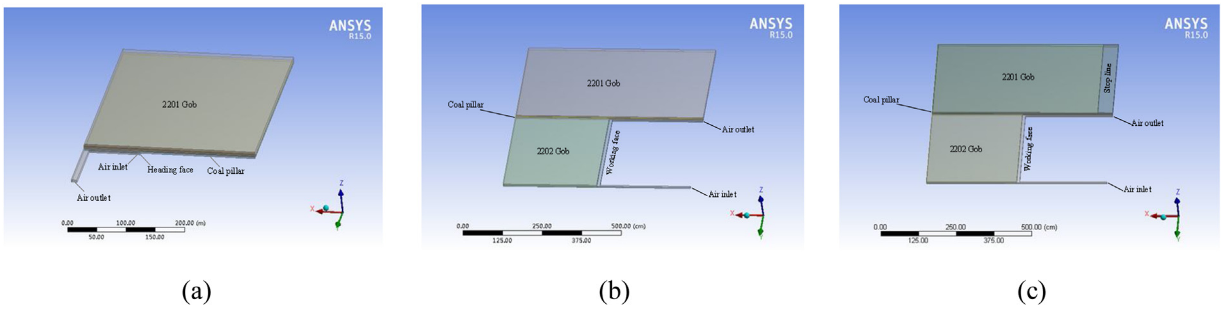

Fig. 4. Calculation model of 2202 working face in three different mining stages.

Table 3
Simulation parameter settings.

Category	Setting conditions
Boundary condition	I model:inlet = Velocity inlet = 0.5 m/s; outlet = outflow II ,III model: inlet = Velocity inlet = 1.7 m/s; outlet = outflow
Velocity inlet	Oxygen mass fraction is 23 %; Nitrogen mass fraction is 77 %
Porosity of gob along the side	p = 0.25
Gob porosity	p = 0.3
Coal wall in Gob	Non-slip velocity condition, u = v = 0
Oxygen consumption rate	User Defined Functions (Su et al., 2016; Huang et al., 2018)

leakage intensity component in their respective directions, m/s; P represents the air leakage pressure, Pa; ρ represents the oxygen density, kg/m^3; g represents the gravitational acceleration, m/s^2; absolute permeability is defined as: $k = K{\cdot}\mu$, m^2; μ represents the air viscosity coefficient, kg/(m·s); K represents the permeability coefficient, m^3·s/kg; D represents the oxygen diffusion coefficient, m^2/s; C represents the oxygen concentration at a certain time, mol·cm^{-3}; C_0 represents the oxygen concentration in the fresh airflow, mol·cm^{-3}; $V(T)$ represents the oxygen consumption rate at a certain time, mol/(cm^3·s); $V_0(T)$ represents the oxygen consumption rate in the fresh airflow, mol/(cm^3·s).

There is a small elevation difference between the air inlet and outlet, where the pressure difference is negligible. The specific settings of the parameters required for the simulation are shown in Table 3.

4. Results and discussion

4.1. Spontaneous coal combustion characteristics

4.1.1. Oxygen consumption rate

The ability of coal samples to consume oxygen can be an important indicator to identify spontaneous coal combustion tendency (Qin et al., 2012; Zhang et al., 2019a). The difference in oxygen concentration at different locations inside the coal pile mainly depends on air convection, diffusion, and oxygen consumption of the coal-oxygen composite reaction. The mathematical expression of oxygen consumption rate is shown in Eq. (6). The oxygen consumption rates of the coal sample during both oxidation processes were calculated from the oxygen concentration and other parameters obtained from experiments. The relation between oxygen consumption rate and oxygen concentration is (Liu et al., 2017a; Zhao et al., 2019):

$$V_0(T) = \frac{\overline{Q} \cdot C_1}{S \cdot L} \cdot \ln \frac{C_1}{C_2} \tag{6}$$

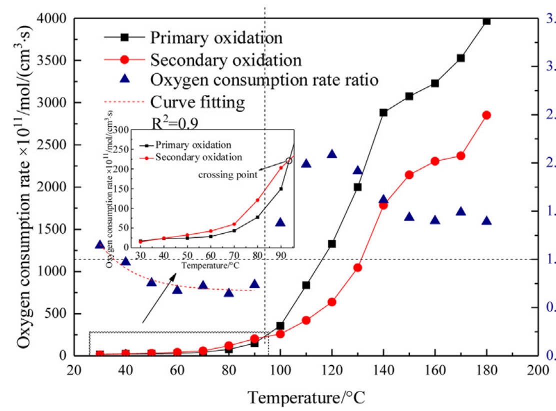

Fig. 5. Fitting curve of oxygen consumption rate ratio during two oxidations.

where $\overline{Q}$ is the gas supply, cm^3/s; S is the tank bottom area, cm^2; L is the coal sample height, cm; C_1 is the oxygen concentration in the inlet of the coal sample tank, mol·cm^{-3}; and C_2 is the oxygen concentration in the outlet of the coal sample tank, mol·cm^{-3}.

According to the experimental results of the two oxidation processes, the oxygen consumption rates of primary and secondary oxidations were defined as V_1 and V_2, respectively, and the ratio of V_1 and V_2 was obtained. The ratio of the oxygen consumption rates of the two oxidation processes is shown in Fig. 5.

Fig. 5 shows that the oxygen consumption rate increased with the increase in temperature. At temperatures below 90 °C, the oxygen consumption rate of the secondary oxidation is greater than that of primary oxidation. The oxygen consumption rates of coal samples were less than 2×10^{-9} mol/(cm^3·s), and the growth tendency was relatively slow. Between 90 °C and 100 °C, there was a crossing point of the oxygen consumption rates between primary and secondary oxidation processes. The results show that the rate of oxygen consumption during the two oxidations of coal samples is abruptly changed at the intersection (i.e. the temperature between 90–100 °C), which is consistent with the result of the literature (Deng et al., 2016a). After the intersection, the oxygen consumption rate of the primary oxidation was greater than that of the secondary oxidation. Between 100 °C and 140 °C, the oxygen consumption rate increased significantly, indicating acceleration of the coal oxidation reaction. When the temperature reached 140 °C, the coal oxidation consumed more supply oxygen, and oxygen deficiency limited the oxidation of coal. As a result, the oxygen consumption rate was still increasing, but at a slower rate.

Below 90 °C, V_1/V_2 was less than 1, and above 90 °C, V_1/V_2 was greater than 1. Below 90 °C, the secondary oxidation was stronger than the primary oxidation; above 90 °C, the secondary oxidation was weaker than the primary oxidation. The moisture of the coal sample was reduced after primary oxidation, and cracks developed in the coal, increasing its porosity and with an increased contact

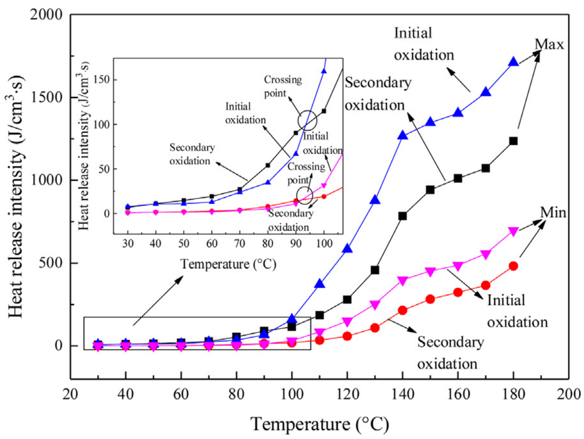

Fig. 6. Relationship between heat release rate and temperature during two oxidations.

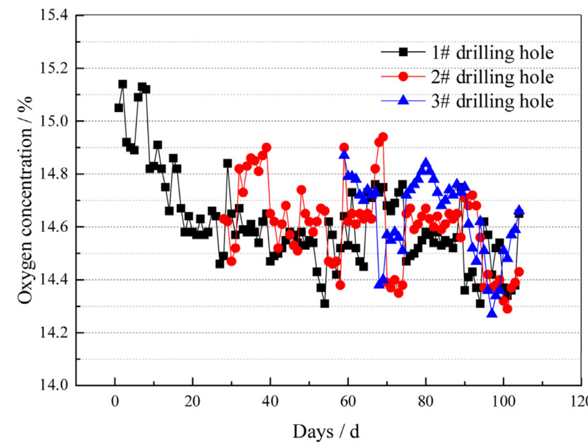

Fig. 7. Monitoring data of boreholes 1, 2, and 3 along gob-side entry during driving period.

area between coal and oxygen. Thus, the oxygen consumption rate was accelerated in the early stage of secondary oxidation. In the later stage of the reaction, the number of active groups participating in the coal-oxygen complex was reduced, resulting in a decrease in oxygen consumption rate.

Considering the importance of the stage before crossing point temperature to coal-oxygen complexation, and providing a reference for the oxygen consumption rate user-defined function of the coal sample in the numerical simulation, the ratio of the oxygen consumption rates for temperatures less than 90 °C was fitted. The fitting degree was approximately 0.9. The mathematical expression is shown as Eq. (7).

$$\bar{y} = 4.24e^{\left(-\bar{x}/13.89\right)} + 0.67 \quad (7)$$

where $\bar{x}$ is the temperature of coal, °C; $\bar{y}$ is the ratio of V_1 and V_2.

4.1.2. Heat release rate

Heat release from the coal–oxygen reaction is the main heat source for coal self-heating, and the heat release rate is a crucial indicator of spontaneous coal combustion. The actual heat release rate is between maximum and minimum value. As shown in Eqs. (8) and (9) (Zhang et al., 2019b):

$$q_{max}(T) = \frac{V^0_{CO}(T)}{V^0_{CO}(T) + V^0_{CO_2}(T)} V_0(T)\,\Delta H^{CO} + \frac{V^0_{CO_2}(T)}{V^0_{CO}(T) + V^0_{CO_2}(T)} V_0(T)\,\Delta H^{CO_2} \quad (8)$$

$$q_{min}(T) = \Delta H^{r}\left[V_0(T) - V^0_{CO}(T) - V^0_{CO_2}(T)\right] + \Delta H^{CO} V^0_{CO}(T) + \Delta H^0_{CO_2} V^0_{CO_2}(T) \quad (9)$$

where $q_{max}(T)$ is the maximum heat release rate, J/cm³·s; and $q_{min}(T)$ is the minimum heat release rate, J/(cm³·s); $V^0_{CO}(T)$ and $V^0_{CO_2}(T)$ are the standard CO production rate and CO_2 production rate, mol/(cm³·s); ΔH^{CO_2} and ΔH^{CO} are the reaction heat of CO_2 and CO, kJ/mol; and ΔH^{r} =58.8 kJ/mol.

Based on the equations, the curves shown in Fig. 6 were obtained. As shown that the maximum and minimum heat release rates increased with the increase in temperature. At the same time, between 90 °C and 100 °C, there was a crossing point of the maximum and minimum heat release rates between primary and secondary oxidation processes. The results showed that the oxidation intensity of secondary oxidation was stronger than that of primary oxidation before the crossing point. When the temperature exceeded the crossing point, the opposite result was displayed.

4.2. Oxygen distribution

During the monitoring period, oxygen concentration was measured in the borehole. Other gases with small concentration values, such as CO, were not included in the analysis. The variation of oxygen concentration in boreholes 1, 2, and 3 during roadway driving along the gob is shown in Fig. 7.

Fig. 7 illustrates that as the depth of advancement of the heading face increased, the oxygen concentration at the 1, 2, and 3 measuring points decreased. The oxygen concentration at the borehole 1 measuring point decreased from 15.05 % to 14.65 %, the oxygen concentration at the borehole 2 measuring point decreased from 14.63 % to 14.43 %, and the oxygen concentration at the borehole 3 measuring point decreased from 14.87 % to 14.66 %. The coal pillar was damaged by rock pressure, creating many cracks that allowed air leakage, resulting in a high oxygen concentration in the adjacent gob.

4.3. Simulation results and analysis

4.3.1. Oxygen distribution under each model

During roadway driving along the gob, local ventilation was adopted because the roadway was not connected. Fig. 8(a) shows that the airflow in the roadway seeped into the adjacent gob due to cracks in the coal pillar generated by rock pressure. The residual coal was exposed to oxygen, which was continuously consumed by physical adsorption, chemical adsorption, and chemical reaction, resulting in lower oxygen concentration farther from the coal pillar in the adjacent gob. Fig. 8(b) shows that the oxygen concentration deeper in the gob gradually decreased. The red area on the air inlet side is wider than on the air return side, because the airflow was affected by diffusion, migration resistance, and the oxidation of residual coal. In the positive z-axis direction, the diffusion region of the oxygen concentration was increased. Compared with Fig. 8(b), it is observed in Fig. 8(c) that the oxygen distribution was similar, but there was a difference in the adjacent gob due to the presence of a stop line, which is prone to backflow when airflow is nearby.

4.3.2. Profile of oxygen distribution under each model

To more intuitively display the oxygen distribution in the three models, the oxygen profiles at different depths in the z and x directions of each model were selected, as shown in Figs. 9 and 10.

The cross-sectional views of oxygen distribution at different depths in the z direction are shown in Fig. 9. It is observed in Fig. 9(a) that as the height in the z direction increased, oxygen continuously penetrated deep into the gob from the coal pillar, and the

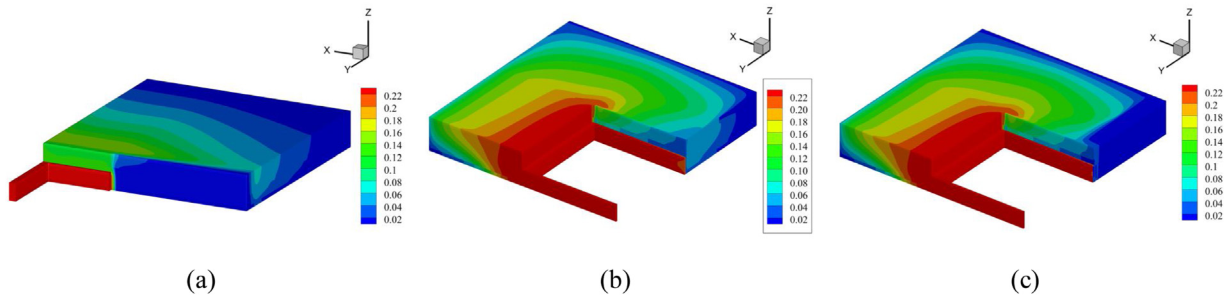

Fig. 8. Oxygen distribution in the gob during: (a) roadway driving along gob; (b) normal mining; (c) end mining.

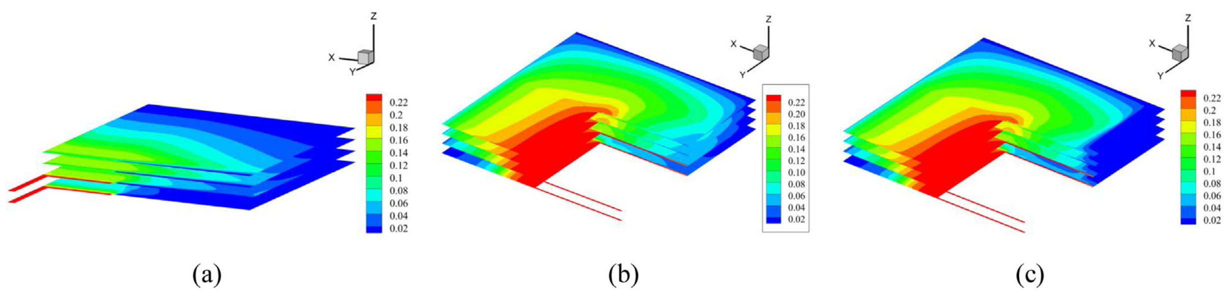

Fig. 9. Oxygen distribution sectional view in the z direction under three different propulsion states.

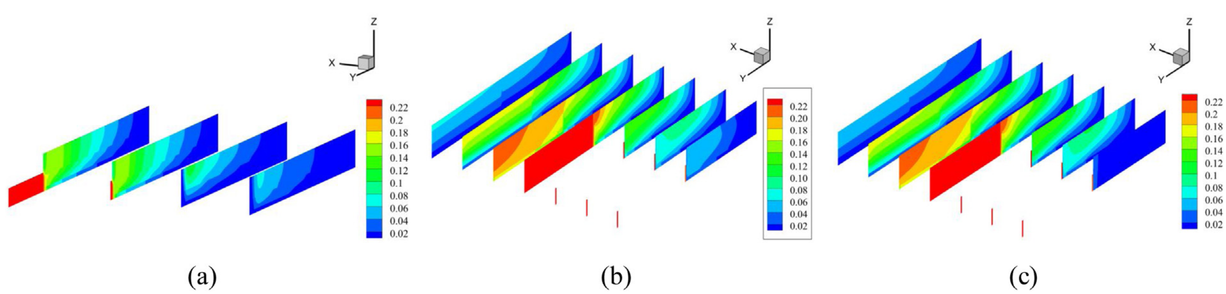

Fig. 10. Oxygen distribution sectional view in the x direction under three different propulsion states.

high-oxygen region continuously expanded. During roadway driving along the gob, oxygen diffused to the adjacent gob behind the heading face, due to air leakage from coal pillars. The highest oxygen mass fraction was 17.9 %. Fig. 9(b) and Fig. 9(c) show that the oxygen concentration on the air inlet side was greater than on the air return side at the same distance from deep in the gob, which is consistent with previous research results (Zhang et al., 2019a). As the height increased, the area of the oxygen region continued to expand, indicating that the underlying coal had consumed significant oxygen, while the overlying rock had not. As cracks in the coal pillar were generated by rock pressure, air leakage resulted in the formation of a long, narrow region of high oxygen content in the adjacent gob near the coal pillar and working face. During mining of the 2202 working face, high oxygen levels and good heat storage conditions were likely to cause continuous oxidation of residual coal, inducing spontaneous combustion. Fig. 9(c) shows the oxygen distribution near the stop line of the 2202 working face, and a disordered airflow due to the stop line in the adjacent gob. The airflow cannot pass through the stop line and several high-speed areas were formed in front of the stop line. The oxygen concentration was less than 2% in the internal stop line.

The cross-sectional views of oxygen distribution at different depths in the x direction are shown in Fig. 10. It is observed in Fig. 10(a) that the oxygen concentration gradually decreased from the coal pillar into the adjacent gob. As the vertical distance increased, the oxygen concentration increased. The oxygen concentration in the direction from the open-off cut to the heading face gradually decreased. The area of the high-oxygen region also decreased. Fig. 10(b) and (c) show that the oxygen concentration gradually decreased deeper in the gob.

4.3.3. *Laws of air leakage intensity*

It is assumed that the air leakage flow in the loose coal along the gob flows in one direction. When the air leakage intensity is constant, the relationship between air leakage intensity and oxygen concentration can be described as (Zhai et al., 2019):

$$Q = \frac{v_0(\theta)(x - x_0)}{c_0 \ln \left(c_0/c\right)} \tag{10}$$

where c and c_0 are the actual oxygen concentration and the standard oxygen concentration (c_0 = 9.375 × 10^{-6} mol/cm^3), respectively; $v_0(\theta)$ is the oxygen consumption rate when the temperature of the loose coal body is θ in the standard oxygen concentration, mol/(cm^3·s); Q is the air leakage intensity, cm^3/(s·cm^2); x and x_0 are the coordinates in the loose coal body and the surface of the roadway, respectively, cm.

According to the oxygen distribution in the numerical simulation of the three models, the law of air leakage intensity in the adjacent gob can be obtained using Eq. (10).

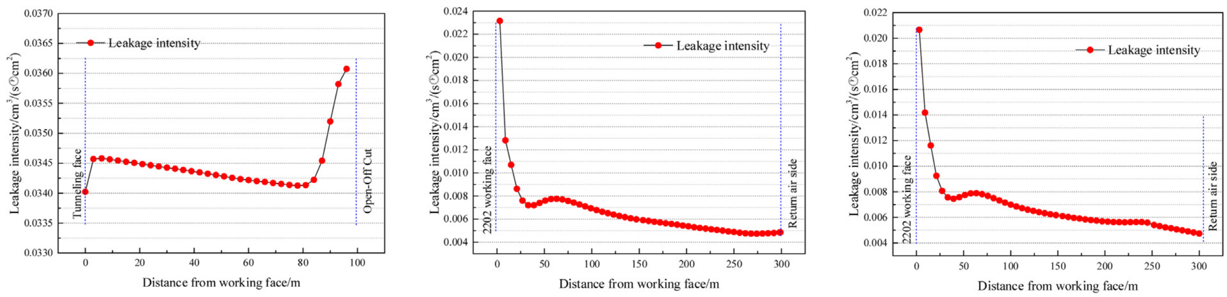

(a) (b) (c)

Fig. 11. Schematic diagram of air leakage intensity inside the coal pillars in adjacent gob.

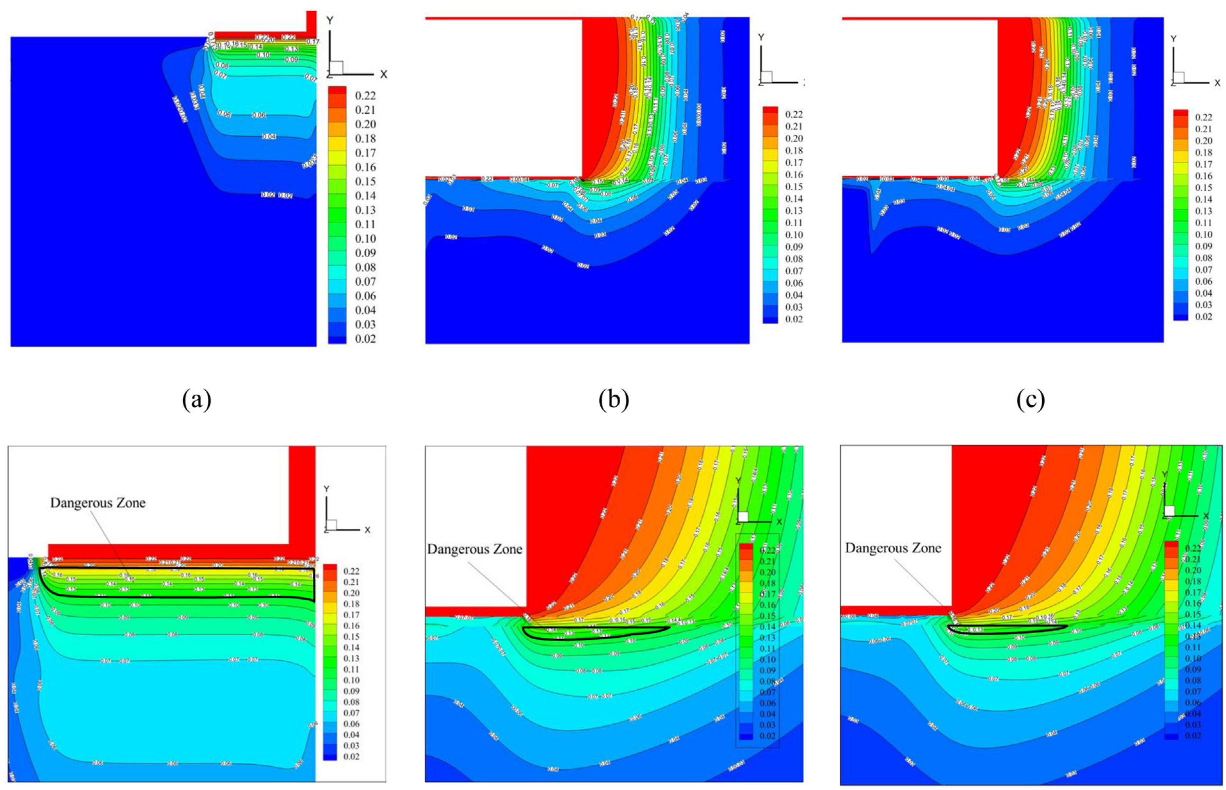

(d) (e) (f)

Fig. 12. Distribution of oxygen concentration in the z = 0.5 plane in three different propulsion states.

To study the spontaneous coal combustion zone in the adjacent gob, it is particularly important to understand the air leakage intensity in the coal pillar. Air leakage from the coal pillar is a significant factor in the high oxygen concentration of the adjacent gob. Fig. 11(a) shows that during roadway driving along the gob of the 2202 working face, the air leakage intensity of the coal pillar along the gob was between 0.0335–0.0365 cm^3/(s·cm^2), and the value remained nearly the same. Fig. 11(b) shows that during normal mining of the 2202 working face, the air leakage intensity of the coal pillar in front of the working face decreased. The air leakage intensity sharply decreased at 15 m in front of the working face. The maximum air leakage intensity of the coal pillar at the working face was 0.024 cm^3/(s·cm^2), approximately six times the value at 300 m in front of the working face. Fig. 11(c) shows that during end mining, the air leakage intensity of the coal pillar in front of the 2202 working face decreased. The air leakage intensity sharply decreased at 15 m in front of the working face. The maximum air leakage intensity of the coal pillar at the working face was 0.0208 cm^3/(s·cm^2), and the minimum air leakage intensity at 300 m in front of the working face was 0.005 cm^3/(s·cm^2). It is observed in Fig. 11 that the air leakage intensity of the coal pillar during roadway driving along the gob is greater than during normal mining and end mining. This is mainly due to the use of push-in local ventilation in roadway driving, and the length of the roadway, which was 100 m. The wind pressure during driving was much greater than during normal mining and end mining.

4.3.4. Classification of hazardous areas under each model

Based on the theoretical knowledge of the' three zones' of spontaneous coal combustion, this study uses oxygen concentration (oxygen volume fraction) as an index to classify the spontaneous coal combustion zone (Huang et al., 2018; Song et al., 2019). An oxygen concentration of 18 % is the critical point between the cooled zone and the spontaneous combustion zone; an oxygen concentration of 10 % is the critical point between the spontaneous combustion zone and the suffocation zone. The planes with vertical direction z = 0.5 m in the three models were selected, and risk zones were classified according to their oxygen concentration. Fig. 12(a–c) are overall schematic views of the three models, and Fig. 12(d–f) are partial enlarged views of the three models.

As shown in Fig. 12(a) and (d), during roadway driving along the gob of the 2202 working face, the oxygen concentration on the coal pillar side of the adjacent gob behind the heading face of Model I is relatively high. The oxygen volume fraction in the area 23 m behind the heading face to the depth of the adjacent gob was between 10 % and 18 %, which is considered to be the spontaneous coal combustion zone. The area at the heading face was narrow, while the area of the open-off cut was wide. It is shown in Figs. 12(b) and (e) that during normal mining there was a long, narrow region of high oxygen near the 2202 working face and coal pillar in the adjacent gob of Model II. This region had an oxygen volume fraction ranging from 10 % to 18 % along the coal pillar from 14 m in front of the 2202 working face to 73 m behind the working face. Its maximum width was 15 m, and its minimum width occurred 73 m behind the working face. Fig. 12(c) and (f) show a similar long, narrow region of high oxygen during end mining in the adjacent gob of Model III. This region had an oxygen volume fraction ranging from 10 % to 18 % along the coal pillar from 12 m in front of the 2202 working face to 74 m behind the working face. Its maximum width was 16 m, and its minimum width occurred 74 m behind the working face. An area of residual coal approximately 87 m in length in the adjacent gob was in a high oxygen environment for a significant time. When the advancing speed of the working face was slow, the residual coal in this area was prone to oxidation. If heat storage conditions for combustion were met, the coal was at risk of fire.

5. Conclusion

In this work, coal oxidation experiment, site monitoring, and numerical simulation were applied to investigate the risk zone of spontaneous coal combustion in the adjacent gob during different stages of coal mining. This work has certain guiding significance for the theoretical research and prevention of spontaneous coal combustion in coal mines. Based on the results, the following conclusions can be drawn:

1 Through two temperature-programmed oxidation experiments, it was found that below 90 °C, secondary oxidation of coal samples was stronger than primary oxidation; above 90 °C, primary oxidation was stronger than secondary oxidation. The ratio of oxygen consumption rates of coal samples during the two oxidation processes below 90 °C was fitted to obtain the relationship.
2 Air leakage of coal pillars was a primary cause of high oxygen in the adjacent gob. During roadway driving along the gob of the 2202 working face, the air leakage intensity of the coal pillar along the gob was between 0.0335–0.0365 $cm^3/(s\cdot cm^2)$. During normal mining and end mining, the air leakage intensity of the coal pillar along the gob was between 0.005–0.024 $cm^3/(s\cdot cm^2)$.
3 During roadway driving along the gob of the 2202 working face, the area 23 m behind the heading face to the depth of the adjacent gob was considered to be the spontaneous coal combustion zone. During normal mining and end mining, an area of residual coal 87 m long in the adjacent gob was in a high-oxygen environment for an extended period of time. When the working face advanced slowly, the residual coal in this area was susceptible to oxidation. Given heat storage conditions necessary for combustion, the coal was easily ignited, threatening the safety of the mine.

Declaration of Competing Interest

The authors declare that they have no conflicts of interest.

Acknowledgements

This work was supported by the National Natural Science Foundation of China (Nos. 5150−4190, and 5150−4186), and the National Key R&D Program of China (No. 2018YFC0808104), and the Key Research and Development Program of Shaanxi Province, China (No. 2017ZDCXL-GY-01-02-03).

References

Bai, Z.J., Wang, C.P., Deng, J., Kang, F.R., Shu, C.M., 2020a. Experimental investigation on using ionic liquid to control spontaneous combustion of lignite. Process. Saf. Environ. Prot, http://dx.doi.org/10.1016/j.psep.2020.06.017.
Bai, Z.J., Wang, C.P., Deng, J., Kang, F.R., Shu, C.M., 2020b. Effects of ionic liquids on the chemical structure and exothermic properties of lignite. J. Mol. Liq., http://dx.doi.org/10.1016/j.molliq.2020.113019.
Cheng, J.W., Yang, S.Q., 2012. Data mining applications in evaluating mine ventilation system. Saf. Sci. 50 (4), 918–922.
Deng, J., Zhao, J.Y., Zhang, Y.N., Huang, A.C., Liu, X.R., Zhai, X.W., Wang, C.P., 2016a. Thermal analysis of spontaneous combustion behavior of partially oxidized coal. Process. Saf. Environ. Prot. 104, 218–224.
Deng, J., Zhao, J.Y., Zhang, Y.N., Wang, C.P., 2016b. Micro-characteristics of spontaneous combustion of second oxidation with different rank coals. Journal of the China Coal Society. 41 (5), 1164–1172.
Deng, J., Lei, C.K., Xiao, Y., et al., 2018a. Determination and prediction on "three zones" of coal spontaneous combustion in a gob of fully mechanized caving face. Fuel 211, 458–470.
Deng, J., Ren, L.F., Ma, L., Lei, C.K., Wei, G.M., Wang, W.F., 2018b. Effect of oxygen concentration on low-temperature exothermic oxidation of pulverized coal. Thermochim. Acta 667, 102–110.
Gao, F.Q., Stead, D., Kang, H.P., Wu, Y.Z., 2014. Discrete element modelling of deformation and damage of a roadway driven along an unstable goaf — A case study. Int. J. Coal Geol. 127, 100–110.
Guo, J., Wen, H., Zheng, X.Z., Liu, Y., Cheng, X.J., 2019. A method for evaluating the spontaneous combustion of coal by monitoring various gases. Process. Saf. Environ. Prot. 126, 223–231.
Huang, Z.A., Ma, Z.Z., Song, S.Y., Yang, R., Gao, Y.K., Zhang, Y.H., 2018. Study on the influence of periodic weighting on the spontaneous combustion "three-zone" in a gob. J. Loss Prev. Process Ind. 55, 480–491.
Kuenzer, C., Zhang, J.Z., Tetzlaff, A., Dijk, P.V., Voigt, S., Mehl, H., Wagner, W., 2007. Uncontrolled coal fires and their environmental impacts: investigating two arid mining regions in north-central China. Appl. Geogr. 27 (1), 42–62.
Lei, C.K., Deng, J., Cao, K., Ma, L., Xiao, Y., Ren, L.F., 2018. A random forest approach for predicting coal spontaneous combustion. Fuel 223, 63–73.
Li, J.H., Li, Z.H., Yang, Y.L., Wang, C.J., 2018. Study on oxidation and gas release of active sites after low-temperature pyrolysis of coal. Fuel 233, 237–246.
Liang, Y.T., Wang, S.G., 2017. Prediction of coal mine goaf self-heating with fluid dynamics in porous media. Fire Saf. J. 87, 49–56.
Liang, Y.T., Zhang, J., Wang, L.C., Luo, H.Z., Ren, T., 2019. Forecasting spontaneous combustion of coal in underground coal mines by index gases: a review. J. Loss Prev. Process Ind. 57, 208–222.
Liu, W., Qin, Y.P., 2017a. A quantitative approach to evaluate risks of spontaneous combustion in long wall gobs based on CO emissions at upper corner. Fuel 210, 359–370.
Liu, W., Qin, Y.P., 2017b. Multi-physics coupling model of coal spontaneous combustion in longwall gob area based on moving coordinates. Fuel 188, 553–566.
Lu, Y., Qin, B.T., 2015. Identification and control of spontaneous combustion of coal pillars: a case study in the Qianyingzi Mine, China. Nat. Hazards 75 (3), 2683–2697.
Ma, L., Guo, R.Z., Gao, Y., Ren, L.F., Wei, G.M., Li, C.H., 2019. Study on coal spontaneous combustion characteristics under methane-containing atmosphere. Combust. Sci. Technol. 191 (8), 1456–1472.
Pan, R.K., Lu, C., Yang, K., Yu, M.G., 2011. Distribution regularity and numerical simulation study on the coal spontaneous combustion "three zones" under the ventilation type of ventilation type of Ч +. J. Procedia Engineering 26, 704–711.
Qin, Y.P., Liu, W., Yang, C., Fan, Z.Z., Wang, L.L., Jia, G.W., 2012. Experimental study on oxygen consumption rate of residual coal in goaf. Saf. Sci. 50 (4), 787–791.
Querol, X., Zhuang, X., Font, O., Izquierdo, M., Alastuey, A., et al., 2011. Influence of soil cover on reducing the environmental impact of spontaneous coal combustion in coal waste gobs: a review and new experimental data. Int. J. Coal Geol. 85, 2–22.
Ren, L.F., Deng, J., Li, Q.W., Ma, L., Zou, L., Laiwang, B., Shu, C.M., 2019. Low-temperature exothermic oxidation characteristics and spontaneous combustion risk of coal. Fuel 252, 238–245.
Rosema, A., Guan, H., Veld, H., 2001. Simulation of spontaneous combustion, to study the causes of coal fires in the Rujigou Basin. Fuel 80, 7–16.

Shi, G.Q., Ding, P.X., Guo, Z.X., Wang, Y.M., 2019. Modeling temperature distribution upon liquid-nitrogen injection into a self heating coal mine goaf. Process. Saf. Environ. Prot. 126, 278–286.
Song, Z.Y., Zhu, H.Q., Tan, B., Wang, H.Y., Qin, X.F., 2014. Numerical study on effects of air leakages from abandoned galleries on hill-side coal fires. Fire Saf. J. 69, 99–110.
Song, Y.W., Yang, S.Q., Hu, X.C., Song, W.X., Sang, N.W., Cai, J.W., Xu, Q., 2019. Prediction of gas and coal spontaneous combustion coexisting disaster through the chaotic characteristic analysis of gas indexes in goaf gas extraction. Process. Saf. Environ. Prot. 129, 8–16.
Su, H.T., Zhou, F.B., Song, X.L., Shi, B.B., Sun, S.H., 2016. Risk analysis of coal self-ignition in longwall gob: A modeling study on three-dimensional hazard zones. Fire Saf. J. 83, 54–65.
Su, H.T., Zhou, F.B., Song, X.L., Qiang, Z.Y., 2017. Risk analysis of spontaneous coal combustion in steeply inclined longwall gobs using a scaled-down experimental set-up. Process. Saf. Environ. Prot. 111, 1–12.
Tang, Y.B., Wang, H.E., 2019. Experimental investigation on microstructure evolution and spontaneous combustion properties of secondary oxidation of lignite. Process. Saf. Environ. Prot. 124, 143–150.
Tang, M.Y., Jiang, B.Y., Zhang, R.Q., Yin, Z.Q., Dai, G.L., 2016. Numerical analysis on the influence of gas extraction on air leakage in the gob. J. Nat. Gas Sci. Eng. 33, 278–286.
Wang, Jf., Zhang, Y.L., Xue, S., Wu, J.M., Tang, Y.B., Chang, L.P., 2018. Assessment of spontaneous combustion status of coal based on relationships between oxygen consumption and gaseous product emissions. Fuel Process. Technol. 179, 60–71.
Wessling, S., Kessels, W., Schmidt, M., Krause, U., 2010. Investigating dynamic underground coal fires by means of numerical simulation. Geophys. J. R. Astron. Soc. 172 (1), 439–454.
Widiatmojo, A., Sasaki, K., Sugai, Y., Suzuki, Y., Tanaka, H., Uchida, K., Matsumoto, H., 2015. Assessment of air dispersion characteristic in underground mine ventilation: field measurement and numerical evaluation. Process. Saf. Environ. Prot. 93, 173–181.
Wu, J.J., Liu, X.C., 2011. Risk assessment of underground coal fire development at regional scale. Int. J. Coal Geol. 86 (1), 87–94.
Xi, Z.L., Li, D., Feng, Z.Y., 2017. Characteristics of polymorphic foam for inhibiting spontaneous coal combustion. Fuel 206, 334–341.
Yang, Y.L., Li, Z.H., Tang, Y.B., Liu, Z., Ji, H.J., 2014. Fine coal covering for preventing spontaneous combustion of coal pile. Nat. Hazards 74 (2), 603–622.
Yuan, L.M., Smith, A.C., 2012. The effect of ventilation on spontaneous heating of coal. J. Loss Prev. Process Ind. 25 (1), 131–137.
Zhai, X.W., Deng, J., Wen, H., Ma, W., 2011. Research of the air leakage law and control techniques of the spontaneous combustion dangerous zone of re-mining coal body. Procedia Eng. 26, 472–479.
Zhai, X.W., Wang, B., Jiang, S.R., Zhang, W.X., 2019. Oxygen distribution and air leakage law in gob of working face of U+L ventilation system. Math. Probl. Eng. 2019, 1–10.
Zhang, J., Zhang, H.T., Ren, T., 2019a. Proactive inertisation in longwall goaf for coal spontaneous combustion control-A CFD approach. Saf. Sci. 113, 445–460.
Zhang, Y.N., Chen, L., Zhao, J.Y., Deng, J., Yang, H., 2019b. Evaluation of the spontaneous combustion characteristics of coal of different metamorphic degrees based on a temperature-programmed oil bath experimental system. J. Loss Prev. Process Ind. 60, 17–27.
Zhao, J.Y., Deng, J., Song, J.J., Shu, C.M., 2019. Effectiveness of a high-temperature-programmed experimental system in simulating particle size effects on hazardous gas emissions in bituminous coal. Saf. Sci. 115, 353–361.
Zheng, X.Z., Deng, J., Zhang, D., Wen, H., 2019. Design and performance of a novel foaming device for plugging air leakage in underground coal mines. Powder Technol. 344, 842–848.
Zhou, H., Qin, B.T., Qin, Q.H., Su, Z.W., 2019. Modeling and simulation of coal spontaneous combustion in a gob of shallow buried coal seams. Process. Saf. Environ. Prot. 131, 246–254.
Zhu, J.F., He, N., Li, D.J., 2012. The relationship between oxygen consumption rate and temperature during coal spontaneous combustion. Saf. Sci. 50 (4), 842–845.
Zhuo, H., Qin, B.T., Qin, Q.H., Su, Z.W., 2019. Modeling and simulation of coal spontaneous combustion in a gob of shallow buried coal seams. Process. Saf. Environ. Prot. 131, 246–254.